TOWARDS OIL SLICK MONITORING IN THE ARCTIC ENVIRONMENT

Camilla Brekke[(1)], **Benjamin Holt**[(2)], **Cathleen Jones**[(2)] **and Stine Skrunes**[(1)]

[(1)]*Department of Physics and Technology, University of Tromsø, Norway, Email:camilla.brekke@uit.no*
[(2)] *Jet Propulsion Laboratory, California Institute of Technology, Pasadena, California, USA*

ABSTRACT

We investigate the potential of multi-polarization and multi-frequency SAR systems to discriminate oil-in-sea-ice mixtures from newly frozen and young sea ice. The dielectric properties of oil emulsions, for a range of oil volume fractions, and theoretical co-polarization ratios for relevant media are modeled and discussed. We also compare the co-polarization ratios computed from actual detected oil spills in the Gulf of Mexico and the North Sea with available collections of sea ice data from the Arctic region. The results show promise for the purpose of SAR being used to separate oil-in-sea-ice emulsions from newly frozen ice-covered Arctic sea water.

1. INTRODUCTION

The reduction in extent and thickness of the Arctic sea ice makes new shipping routes and natural resources more easily accessible at high latitudes. Increased activity is expected in the Arctic regions from the international maritime industry and the oil and gas sector in the coming years. New knowledge on and development of technology for oil spill remote sensing in Arctic conditions are needed to address the increased risk. To the authors' knowledge, there are few existing publications on this topic [13, 2].

This study is at a preliminary stage, with the focus currently on thin sea ice features (new lead ice, grease ice and thin young ice) that appear dark in synthetic aperture radar (SAR) imagery. Thin sea ice, low wind regions and biogenic slicks are examples of low backscattering phenomena that could resemble oil slicks in the marginal ice zone, and hence cause false oil spill alarms in SAR observations.

New/young sea ice types have similar radar backscatter signatures to those of oil and thus may be difficult to separate. Our work is a theoretical investigation of the potential of multi-polarization and multi-frequency SAR data to discriminate look-alikes from oil spills in icy waters. We pursue this by comparing actual detected oil spills, e.g., in the Gulf of Mexico and the North Sea, with available collections of sea ice data from the Arctic region. To support the data analysis, results from a theoretical study on the relative permittivity of oil-in-sea-ice mixtures are discussed.

For our study, we focus on the co-polarization ratio, defined as the ratio of the radar cross sections from polarization-preserving scattering (VV/HH, where the first (second) letter indicates the polarization of the incident (scattered) radiation, either horizontal or vertical). Within the Bragg scattering model, this quantity is a function of the complex dielectric constant of the medium and the incidence angle, and is observed to be large for both open water and new sea ice.

NASA AIRSAR scenes recorded from the Beaufort Sea, containing multiple recently frozen sea ice leads [1] are investigated. Our analysis of the co-polarization ratio indicates a benefit of combining multi-polarization and multi-frequency measurements for discrimination among various thin sea ice classes.

State-of-the-art knowledge on oil slick characterization by current polarimetric radar systems, such as NASA's UAVSAR, RADARSAT-2, and TerraSAR-X, is used as a reference in this work [12, 15, 16]. The co-polarization ratio of both biogenic slicks and mineral slicks is observed to be lower than open sea water. We also expect new, young and thin sea ice to have dielectric properties closer to open sea water. Hence, it therefore seems appropriate to investigate the potential of discriminating oil-in-sea-ice mixtures from new/thin ice using polarimetric SAR.

Section 2 discusses the dielectric properties of open sea, sea ice and oil, and preliminary modeling of oil mixed in newly frozen sea ice. Section 3 discusses the scattering matrix for a Bragg surface and theoretical analysis of the co-polarization ratio of relevant dielectric media. Experimental results based on AIRSAR, RADARSAT-2 and UAVSAR data are presented and discussed in Sections 4, 5 and 6, while preliminary conclusions are drawn in Section 7.

2. DIELECTRIC PROPERTIES

For SAR remote sensing of oil slicks in Arctic waters, a physical parameter of interest is the complex dielectric constant of mixtures of oil and sea water, i.e., emulsions, at the freezing point. Modeling this parameter requires information on

the dielectric properties of both the unmixed oil and the unmixed sea ice.

2.1 Complex relative permittivity

The relative permittivity, or the complex dielectric constant, is a complex number defined as $\varepsilon = \varepsilon' - i\varepsilon''$, where $i = \sqrt{-1}$, ε' is the real permittivity of the material and ε'' is the dielectric loss factor of the material. The real permittivity measures the linear response of a material to an applied electric field and the attenuation of the amplitude of an electromagnetic wave within the medium is a function of the loss factor and, especially for poor conductors, the real permittivity [8].

2.2 Arctic sea ice

The principal components of first-year sea ice are solid ice crystals and brine, i.e., a solution of salt in water, both obeying the Debye equation [14]. We are particularly interested in newly frozen ice types. New ice includes frazil ice, grease ice, slush and shuga, while young ice is ice in the transition between nilas and first-year ice [18]. Due to a lack of literature on the dielectric properties of the individual young ice types, we apply what is known about the general dielectric properties of new ice, young ice and first year ice.

From [4, p. 37], we have an empirical relationship between the dielectric properties of sea ice and the relative brine volume, V_b. The real and imaginary parts of the relative permittivity are given in Tab. 1, where $V_b \leq 70\,‰$. In this work, we assume that the relations in Tab. 1 are representative of both new and young sea ice.

Table 1 Real and imaginary parts of the dielectric properties of sea ice relative to brine volume.

Frequency	ε'	ε''
1 GHz	$3.12 + 0.009 \cdot V_b$	$0.04 + 0.005 \cdot V_b$
4 GHz	$3.05 + 0.0072 \cdot V_b$	$0.02 + 0.0033 \cdot V_b$
10 GHz	$3.0 + 0.012 \cdot V_b$	$0.0 + 0.01 \cdot V_b$

From [17, p. 2048], we have an empirical expression for the volume fraction of brine in sea ice, valid for the temperature range $-0.5°C \geq T \geq -22.9°C$:

$$V_b = 10^{-3} S_i \left(-\frac{49.185}{T} + 0.532 \right) \qquad (1)$$

where S_i is the salinity in ‰ of the sea ice mixture.

2.3 Oil pollution

The relative permittivity of mineral oil has a real part that ranges from 2.2-2.3 and an imaginary part less than 0.02 [12]. To the authors' knowledge, there are few existing publications on the behavior of oil at low temperatures and in icy waters [3, 5]. For hydrocarbons, a typical decrease of the dielectric constant with respect to temperature is reported to be 0.0013% or 0.05% per ˚C [3]. Based on this, we consider the dependence of the relative permittivity of oil on temperature to be negligible.

2.4 Linear mixture modeling of oil in sea ice

We consider sea ice as the host material and we investigate oil-in-sea-ice emulsions for various volumetric fractions of the oil.

Several mixing models for dielectric media exist, see e.g. [5, 7]. In this study we adapt the model by [17, p. 2044]:

$$\varepsilon_m^\alpha = \varepsilon_h^\alpha + v_o(\varepsilon_o^\alpha - \varepsilon_h^\alpha) \qquad (2)$$

where ε_h represents the relative permittivity of unmixed sea ice (the host material), ε_o represents the relative permittivity of the unmixed oil, and v_o is the volume fraction of oil in the mixture. For $\alpha=1$, this model is known as the *linear model.*

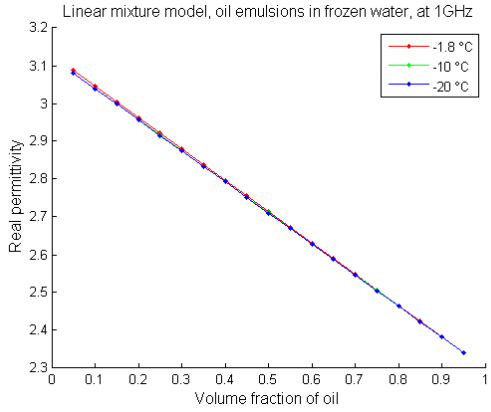

Figure 1 Real permittivity for oil emulsions in frozen water at 1 GHz.

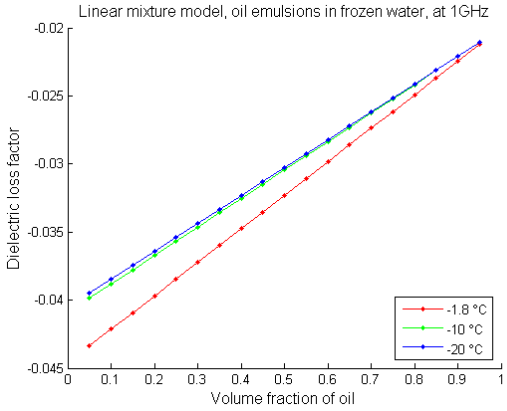

Figure 2 Dielectric loss factor for oil emulsions in frozen water at 1 GHz.

Figs. 1-4 show results from the linear mixture modeling of oil in sea ice, and Tab. 2 summarizes

the unmixed dielectric values used for sea ice and oil as input to the model.

Figs. 1-2 presents the real and imaginary parts of the relative permittivity for the oil-sea ice mixture at 1 GHz. Plots are given for a range of temperatures, at and below the freezing point of sea water in the Arctic which is nominally -1.8 ˚C at a salinity of 33 ‰. In Fig. 1, the real part changes little with temperature, but it is moderately affected by the volume fraction of oil in the mixture. Adding more oil in the mixture lowers the real part of the dielectric constant, which will tend to increase penetration. In Fig. 2, the loss factor, represented by the imaginary part, seems to be slightly less negative for temperatures significantly below the freezing point. The increase in loss factor with higher oil volume, points to less attenuation of the signal within the medium.

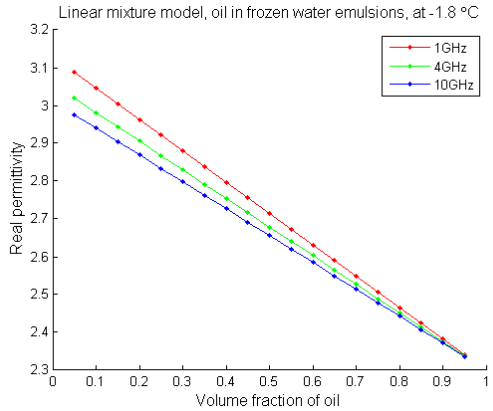

Figure 3 Real permittivity for oil emulsions in frozen water at -1.8 ˚C.

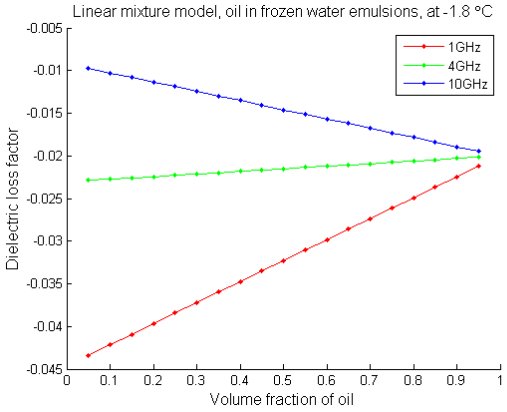

Figure 4 Dielectric loss factor for oil emulsions in frozen water at -1.8 ˚C.

Table 2 Dielectric values of sea ice, adapted from [4, p. 37] and [17, p. 2048], and unmixed oil [12].

Oil	Ice 1 GHz	Ice 4 GHz	Ice 10 GHz
2.3-i0.02	3.1209-i0.0405	3.0507-i0.0203	3.0012-i0.0010

Figs. 3-4 show the real and imaginary part of the relative permittivity for the mixture and various frequencies at the freezing point. In Fig. 3, for all frequencies investigated, it is evident that the real part falls off as a function of increasing volume fraction of oil. With increasing oil content the loss factor in Fig. 4 displays an increase (less negative) at 1 GHz; a very slight increase at 4 GHz; and a decrease (more negative) at 10 GHz. Comparing the loss factor at 1 GHz with that at 4 GHz and 10 GHz, we see an indication of increased penetration into the medium for increased oil volume fractions at 1 GHz. This is due to the observation of the loss factor becoming less negative at this frequency. We also note that the real part in Fig. 3 has a slightly steeper decreasing gradient at 1 GHz compared to 4 GHz and 10 GHz.

3 SURFACE SCATTERING

The scattering matrix for a Bragg surface scatterer (slightly rough surface) on an untilted surface has the following form when the cross-polarized terms are neglected [9]:

$$S = \begin{bmatrix} R_H(\theta, \varepsilon_r) & 0 \\ 0 & R_V(\theta, \varepsilon_r) \end{bmatrix} \tag{3}$$

where

$$R_H(\theta, \varepsilon_r) = \frac{\cos(\theta) - \sqrt{\varepsilon_r - \sin^2(\theta)}}{\cos(\theta) + \sqrt{\varepsilon_r - \sin^2(\theta)}} \quad ,$$

$$R_V(\theta, \varepsilon_r) = \frac{(\varepsilon_r - 1)(\sin^2\theta - \varepsilon_r(1 + \sin^2\theta))}{(\varepsilon_r \cos\theta + \sqrt{\varepsilon_r - \sin^2\theta})^2}$$

and ε_r is the complex relative permittivity of the surface and θ is the incidence angle. Under the reciprocity scattering assumption, the scattering matrix in eq. (3) yields a 3 × 3 surface scattering covariance matrix given by:

$$C_{3\times3} = \begin{bmatrix} |R_H|^2 & 0 & R_H R_V^* \\ 0 & 0 & 0 \\ R_V R_H^* & 0 & |R_V|^2 \end{bmatrix} \tag{4}$$

where * represents the complex conjugate. The covariance matrix is usually estimated from a collection of adjacent pixels.

3.1 Co-polarization ratio

Because of its sensitivity to surface oil, we further investigate the co-polarization ratio, using the approximation $|R_V|^2 / |R_H|^2$. Within the Bragg model, the ratio is independent of roughness,

increases with θ, and is dependent upon the complex relative permittivity of the surface. However, we note that attention should be paid to the range of roughness for which the small-perturbation theory is valid [4, p.426].

Over time in winter, sea ice grows in thickness. The dielectric constant decreases rapidly (from 80 to 11) during the first 5 mm of growth and decreases more slowly as the ice thickness increases to 10 cm [6], eventually reaching a more stable first year ice level. Fig. 5 shows the theoretical co-polarization ratio for selected representative relative permittivity values of oil, open sea water, new ice and young ice. We observe that new ice is closer to sea water while young ice is closer to 50/50 oil-in-sea-ice emulsion and crude oil. We also note that the distinction between the different media becomes more pronounced as the incidence angle increases.

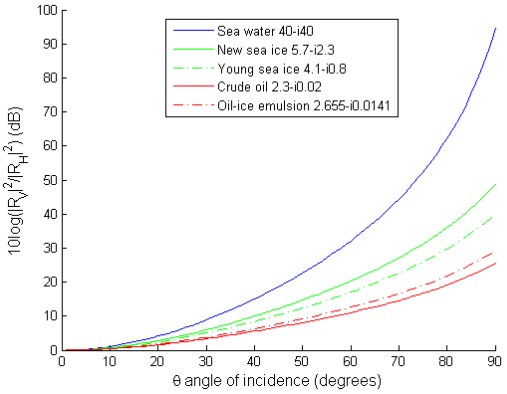

Figure 5 Co-polarization ratios for various representative dielectric media, primarily at 10 GHz. The dielectric properties for sea water are valid for S=35‰, T=0˚C [11]. The dielectric property of crude oil is from [12]; the dielectric property for oil-in-sea-ice 50/50 emulsion is derived for -2 ˚C from the linear mixture model in section 2.4; and the sea ice values are from [6].

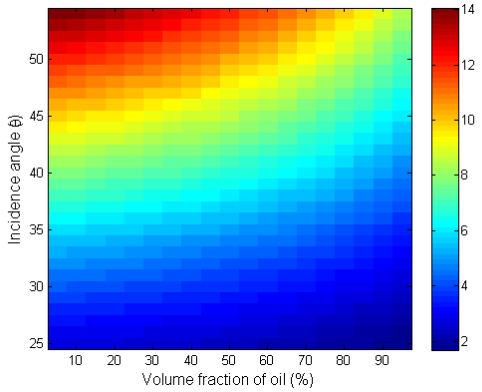

Figure 6 Co-polarization ratio as a function of θ and oil volume fraction in sea ice mixture. Legend in dB.

From Fig. 6, it is clear that smaller oil volume fractions at higher incidence angles will produce higher co-polarization ratios. At lower incidence angles, lower oil volume fractions become indistinguishable from newly frozen sea ice.

Based upon these results, in the following sections we explore the hypothesis that the co-polarization ratio is sensitive to differences in the relative permittivity of sea ice types, sea water and oil to test whether emulsions of oil in newly frozen sea ice can be distinguished from unmixed new ice and young sea ice types.

4 AIRSAR IMAGING OF NEW ICE

Our theoretical analysis of the dielectric properties in section 2 showed that the sensor frequency may play an important role in the ability to detect an oil spill in the Arctic sea ice cover with SAR. We start with a study of AIRSAR multi-frequency polarimetric imagery of newly frozen leads. The data includes a range of recent sea ice types as well as older first year and multiyear ice [1].

The AIRSAR system operated in fully polarimetric mode at P-, L- and C-band simultaneously, and is now retired. In fully polarimetric mode, the instrument transmits and receives pulses of both horizontal (h) and vertical (v) polarization. The AIRSAR system became operational in 1987 and the polarimetric mode became available in 1988.

The noise equivalent sigma nought (NESZ) is a measure of the radar cross-section equivalent to the instrument noise floor and is a function of incidence angle. For AIRSAR, NESZ lies in the range of -32 to -30 dB for C-band, -47 to -43 for L-band and -50 to -49 dB for P-band [10]. Hence, P-band has a lower NESZ compared to L-band and C-band and would therefore be expected to be more sensitive in terms of measurements of dark features. However, P-band is found to be less useful for new lead ice type discrimination, as we report below.

4.1 Ground truth and study site

Table 3 Sea ice types with estimated age and thickness. Age and thickness information from [1].

Ice type and age (days)	Thickness (cm)
Lead ice (<1)	0-9
Lead ice (1-2)	8-13
Lead ice (2-3)	12-15
Lead ice (9-14)	25-36
Thin FY ice	>32

In this study, we have analyzed three AIRSAR scenes that contain sea ice leads, recorded from the Beaufort Sea on 2 December 2004. Fig. 7 shows some of the HH-channel images from two of the scenes, and for different frequencies, labeled with estimated ages of the lead ice types as derived from

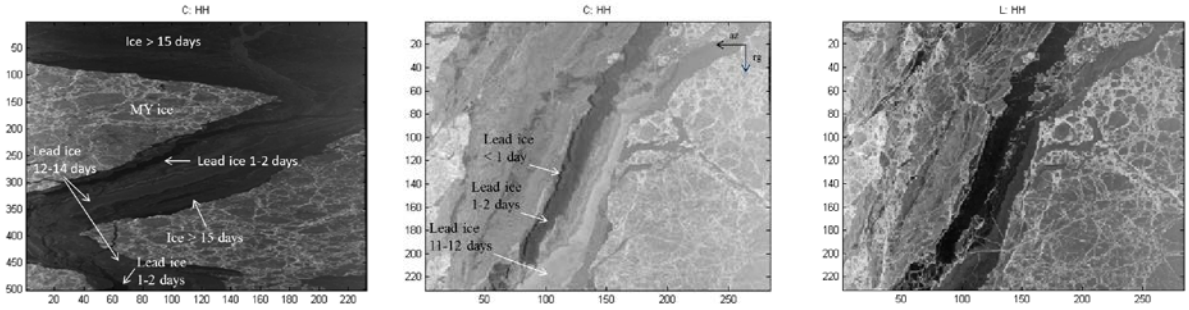

Figure 7 AIRSAR imagery from the Beaufort Sea. Left (scene 6830): Ice type labels overlaid C-band HH channel. Middle and right (scene 6832): Ice type labels overlaid C-band HH (middle). L-band HH (right).

a coincident RADARSAT-1 time series. Tab. 3 defines the sea ice age in terms of type and estimated thickness [1].

4.2 Experimental results

Fig. 8 and Fig. 9 show the co-polarization ratio computed for all AIRSAR frequencies, C-, L-and P-band respectively. The following should be noted: C-band clearly highlights lead ice that is new, <1-3 days old and thin (see Tab. 3). The new lead ice has the highest co-polarization ratio compared to the other sea ice classes present in the scenes. This could be related to a high relative permittivity that is expected for newly frozen sea ice because of its high salinity content.

L-band highlights lead ice types that are a few days older and thicker, e.g., ice labeled as 11-12 days in Fig. 7 (middle) has the highest co-polarization ratio as seen in Fig. 9 (middle). Comparing the images in the middle and to the right in Fig. 7, we see that the 11-12 days lead ice region has bright characteristics in HH-polarization for C-band, while relatively low backscatter for L-band. In addition to high co-polarization ratios, thin ice forming in leads was previously found to cause a significant phase shift between HH and VV channels in L-band frequency [4, p.427]. A phase shift can be related to a finite layer thickness effect that enables interference of top- and bottom-scattered signals. Drinkwater et al. [4, p.427] suggested that the upper ice surface could appear roughened by frost flowers high in salinity. The vertical geometry of frost flowers can alter the polarization dependence of the radar backscatter, changing the co-polarizaton ratio. Although not definitive, this could explain the bright red appearance for L-band in Fig. 9. In both Fig. 8 and Fig. 9, we observe that L-band discriminates better than C-band between multi-year (MY) ice and the young lead ice types.

The results from P-band backscatter are less clear, but give some separation between MY ice and the young lead ice types. As P-band seems less useful for our purpose, this frequency is not discussed further here.

5 NORTH SEA OIL SLICK EXPERIMENT

During the oil-on-water exercise conducted by the Norwegian Clean Seas Association for Operating Companies (NOFO) in June 2011, satellite images of oil spills with corresponding ground truth information such as oil type, volume of the oil released and meteorological condition was collected.

Fig. 10 presents two quad-polarimetric RADARSAT-2 scenes. In the scene on the bottom left, two oil slicks are visible. The slick to the left is 400 L of plant oil, released about 2 hours before image acquisition. The dark region to the right represents 20 000 L of oil emulsion released about 18 hours before the satellite pass. After mechanical recovery, about 1000 L of emulsion remained on the surface. In the image on the top left, three slicks are visible. Furthest to the left is the plant oil slick (13 hours old) and in the middle the emulsion (29 hours old). Furthest to the right is a slick produced from the release of 30 000 L of crude oil about 9 hours before image acquisition. The incidence angle of the scene show on top in Figure 10 lies between 35.1-36.1° with near range to the left. For the scene at the bottom, the incidence angle increases from 46.4° to 47.1° (near range to the right).

A noise analysis has been performed on the image on the top left in Fig. 10, comparing the backscatter levels with the sensor noise floor [15]. Selected regions of 50 by 50 pixels within the different slicks are selected, and the mean sigma zero computed. The mean levels of the plant oil, emulsion and crude oil are found to lie ~9-12 dB, ~5-6 dB and ~3-5 dB above the corresponding NESZ in the co-polarization channels. Several mineral oil regions are less than one standard deviation above the noise floor. For cross-polarization channels, all mean values lie below the noise floor.

In Fig. 10, the co-polarization ratios of the oil slicks are lower than sea water in both cases, which is as expected and according to the theoretical plot in Fig. 5. We also note that no significant difference between plant oil (biogenic slick simulator), emulsion (50/50 mixture at time of release) and crude oil is observed in the co-polarization ratio.

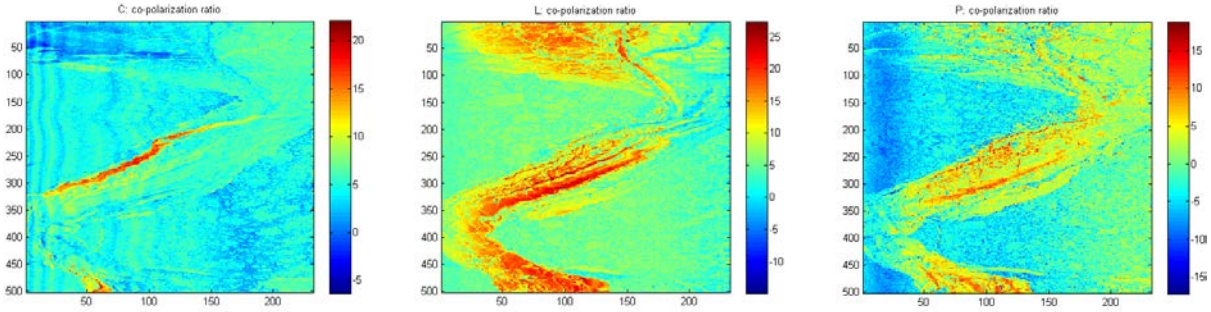

Figure 8 AIRSAR co-polarization ratios (VV/HH). C-, L- and P- band. Scene: 6830. Legends in dB.

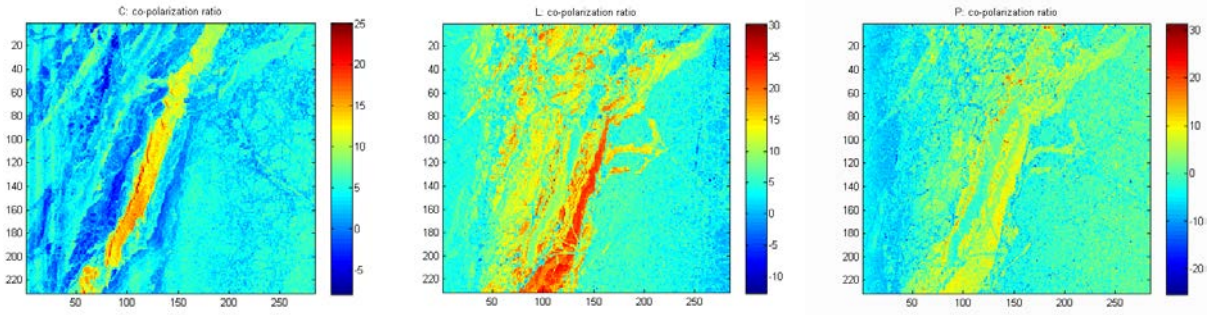

Figure 9 AIRSAR co-polarization ratios (VV/HH). C-, L- and P-band. Scene: 6832. Legends in dB.

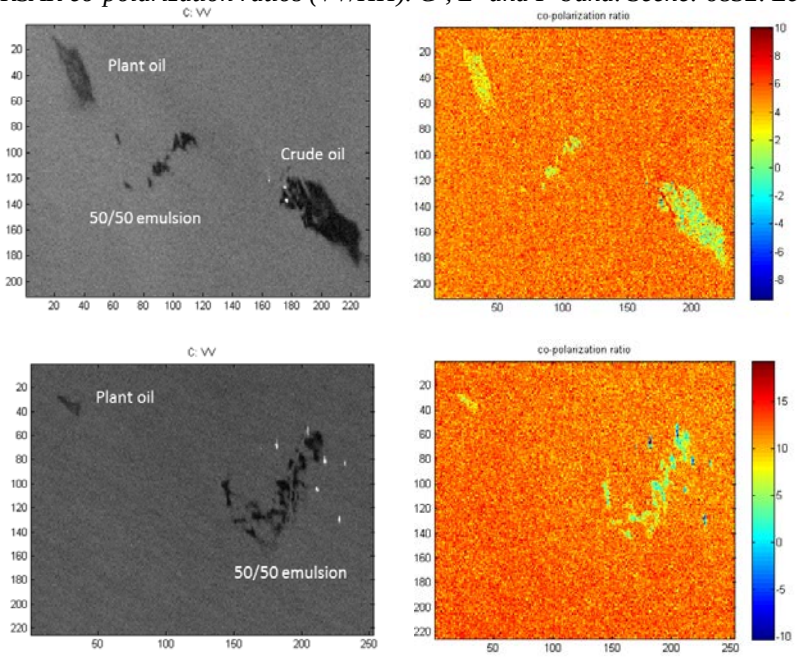

Figure 10 Left: VV channels. Right: Co-polarization ratios (VV/HH) and legend in dB. Wind speed 1 m/s (top) and 6 m/s (bottom). RADARSAT-2 Data and Products© MDA LTD. (2011) - All Rights Reserved.

6 DEEP WATER HORIZON ACCIDENT

UAVSAR is a NASA-operated quad-polarimetric L-band synthetic aperture radar that operates with 80 MHz bandwidth and center frequency 1.2575 GHz. During the Deepwater Horizon oil spill, UAVSAR was deployed in the Gulf of Mexico region on 22-23 June 2010 and collected quad-

polarimetric data over the main slick in the open ocean on 23 June. Previous analysis of the data has shown sensitivity of the L-band backscatter to the oil volumetric fraction [12]. The analysis fit the co-polarization ratio to the tilted Bragg model to estimate the oil fraction for a thick oil-water mixture on the surface. The analysis also showed that the scattering from both the slick and clean water agreed well with the Bragg scattering model across the full incidence angle range from 23-65° for the metrological and surface conditions at the time of imaging, in cases where the backscatter exceeded the instrument noise floor by more than 6 dB. For very low backscatter, the instrument noise contaminated the signal and caused disagreement with the Bragg model.

In Fig. 11 we show the co-polarization ratio (VV/HH) measured with the UAVSAR L-band radar over the main Deepwater Horizon oil slick in the Gulf of Mexico. The figure at top left shows the full image swath with the near range at the top, with the clean water having the larger values and the slick extending across the entire swath in the middle of the image. The incidence angle range shown is 23-65°. The other three images in Fig. 11 are close-ups of locations within the slick (boxes in upper left figure), with the top right showing the up-wind edge of the slick; the bottom left the down-wind edge of the slick, and the bottom right an area of nearly-clear water within the slick. In the close-up images, the oil-slicked waters show up as blue in the chosen colormap. Variations within the slick show clearly in the co-polarization ratio, seen at the slick edges and the convergence zones of the wind-rows. These results show the promise of low-noise SAR for detection of areas with more or less oil for directing response activities.

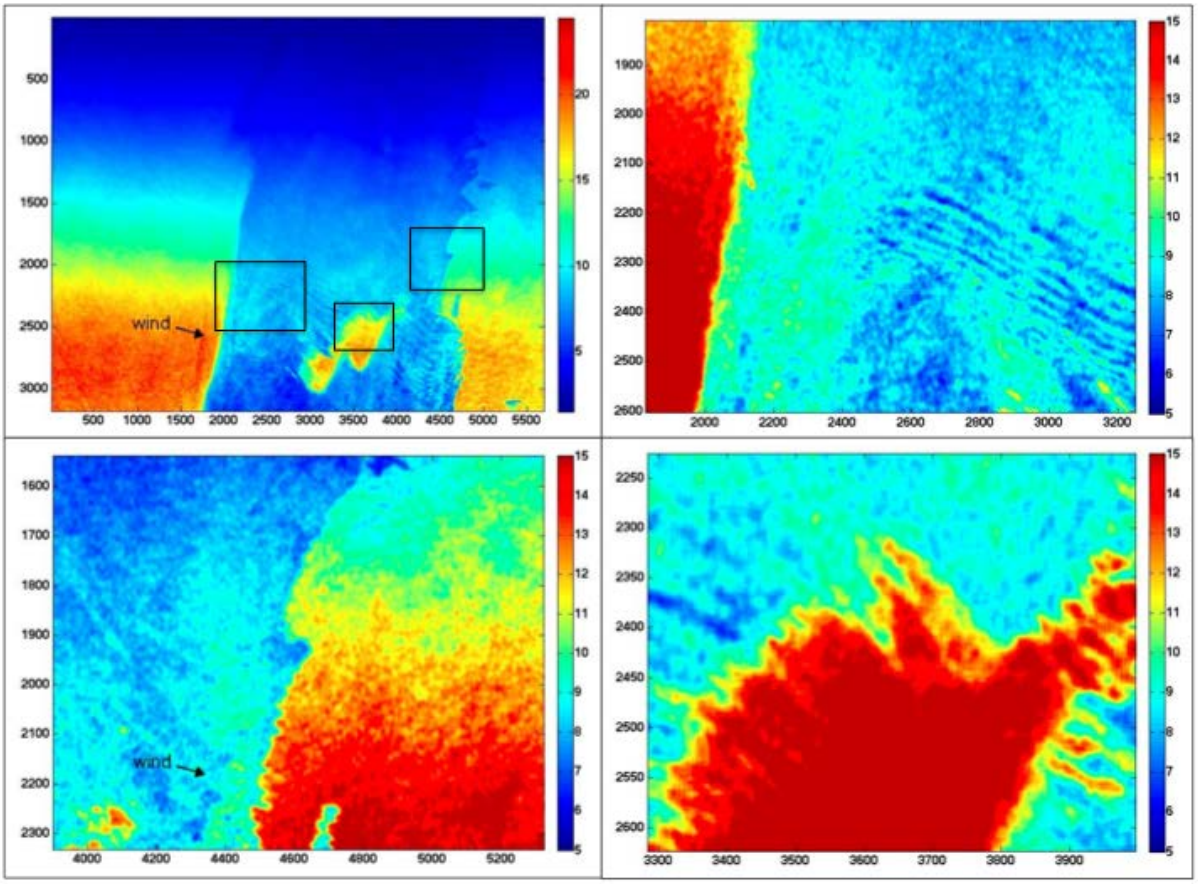

Figure 11 Co-polarization ratios calculated from L-band UAVSAR data collected over the main Deepwater Horizon oil slick in the Gulf of Mexico on 23 June 2010. The figure at the upper left shows the slick across the full 22-km wide image swath (near range at top), surrounded by clean water (red in far range). The other three figures are zoomed images (at different color scales to show the local variation) of several areas within the slick: (upper right) the up-wind edge of the slick and wind-rows within the slick (slick shown in blue); (lower left) the down-wind edge of the slick (slick shown in blue); (lower right) an area of clean water within the slick (slick shown in blue).

7 CONCLUSIONS

Results from a theoretical analysis reveals that oil-in-sea-ice mixtures are expected to have a lower relative permittivity than newly frozen and young sea ice, which approach the values of open sea water at its initial growth stage.

The co-polarization ratio is investigated, as it is independent of roughness and only depends on the incidence angle and the complex relative permittivity of the medium. For C-band SAR imagery, the co-polarization ratio is indeed seen to discriminate between newly frozen sea surfaces (higher relative permittivity) and slightly older new and young ice (lower relative permittivity). C-band SAR measurements collected during a large scale experiment with oil released on open water also show that the co-polarization ratio is significantly lower for 50/50 oil emulsion, plant oil and crude oil as compared to open sea water. These observations seem promising for the purpose of SAR being used to discriminate oil-in-sea-ice emulsions from newly frozen ice-covered Arctic sea water.

Our theoretical modeling of the dielectric properties of mixtures show that the microwave frequency of 1 GHz (L-band) in particular has potential for oil-in-sea-ice emulsions studies, due to the expected greater penetration depth into the mixture as a function of increasing oil volume fraction (real part decrease and imaginary part becomes less negative). However, our experimental results on L-band SAR data of newly frozen lead ice in the Beaufort Sea reveals a potential problem in discriminating very young sea ice from sea ice that is 1-2 weeks old. This problem could be caused by frost flowers that occur during winter in the upper ice surface at high salinity conditions. How this would affect the use of L-band for detecting potential oil spills in the Arctic needs further investigation.

REFERENCES

[1] Bäck, D., "*Analysis of Polarimetric Signatures of Arctic Lead Ice Using Data from AIRSAR and RADARSAT*", MSc Thesis, Dep. of Radio and Space Science, Chalmers Univ. of Tech., Göteborg, Sweden 2008.

[2] Bradford, J. H., Dickins, D. F., and Brandvik, P. J., "Assessing the potential to detect oil spills in and under snow using airborne ground-penetrating radar", *Geophysics*, Vol. 75, No. 2, March-April 2010.

[3] Carey, A. A. and Hayzen, A. J., "*The Dielectric Constant and Oil Analysis*", Practicing oil analysis, Sept. 2001.

[4] Carsey, F. D. (Ed.) "*Microwave Remote Sensing of Sea Ice*", AGU Geophysical Monograph 68, 1992.

[5] Chapman, I. D., "*The Effect of Temperature on Dielectric Properties of Water-in-Oil Emulsions*", *J. Phys. Chem.*, Vol. 72, No. 1, Jan. 1968.

[6] Germain, K. "*Applications on Spectral Microwave Radiometry to Sensing of Sea Ice and the Ocean Surface*", PhD Thesis, Univ. of Massachusetts, May 1993.

[7] Hanai, T. and Koizumi, N., "*Dielectric Constants of Emulsions*", 1962. Available online: http:// repository.kulib.kyoto-u.ac.jp/dspace/bitstream/2433/ 75898/1/chd040_4_240.pdf

[8] Jackson, J. D., "*Classical Electrodynamics*", John Wiley & Sons, Inc., 1962.

[9] Lee, J.-S. and Pottier, E., "*Polarimetric Radar Imaging. From Basics to Applications.*", CRC Press Taylor & Francis Group, 2009.

[10] Lou, Y., "*How Accurate Are My AIRSAR Data?*", in Proc. of AIRSAR Earth Sci. and Appl. Workshop, 2002. Available online: http://airsar.jpl.nasa.gov/documents/ workshop2002/papers/Q5.pdf.

[11] Meissner, T. and Wentz, F. J. "The Complex Dielectric Constant of Pure and Sea Water From Microwave Satellite Observations", *IEEE Trans. on Geosci. and Remote Sensing*, Vol. 42, No. 9, Sept. 2004.

[12] Minchew, B., Jones, C. E., Holt, B., "Polarimetric Analysis of Backscatter From the Deepwater Horizon Oil Spill Using L-Band Synthetic Aperture Radar", *IEEE Trans. of Geosci. and Remote Sensing*, Vol. 50, No. 10, Oct. 2012.

[13] Praks, J., Eskelinen, M., Pulliainen, J., Pyhälahti, T., and Hallikainen, M., "*Detection of oil pollution on sea ice with airborne and spaceborne spectrometer*", in proc. of IGARSS 2004.

[14] Pringle, D. and Ingham, M., "Thermal, Electrical and Hydraulic Properties of Sea Ice", cp. 3.4 in *Field Techniques for Sea Ice Research*, 2009.

[15] Skrunes, S., Brekke, C., Eltoft, T., "Detection of Ocean Surface Slicks in Multi-Polarization C- and X-band SAR Imagery", submitted *IEEE Trans. on Geosci. and Remote Sensing* 2012.

[16] Skrunes, S., Brekke, C., Eltoft, T., "Characterization of Ocean Surface Slicks by Multi-Polarization C- and X-band SAR Imagery", submitted *IEEE Trans. on Geosci. and Remote Sensing* 2012.

[17] Ulaby, F. T., Moore, R. K., and Fung, A. K, "*Microwave Remote Sensing Active and Passive*", Artech House, Inc., 1986.

[18] WMO sea-ice nomenclature, WMO/OMM/MBO-No.259 Suppl.No.5, Linguistic equivalents.